Atomic size and chemical effects on the local order of Zr_2M (M=Co, Ni, Cu, and Ag) binary liquids

Li Huang,[1] C. Z. Wang,[1,2] S. G. Hao,[1] M. J. Kramer,[1,3] and K. M. Ho[1,2]
[1]*Ames Laboratory, U.S. Department of Energy, Ames, Iowa 50011, USA*
[2]*Department of Physics, Iowa State University, Ames, Iowa 50011, USA*
[3]*Department of Materials Science and Engineering, Iowa State University, Ames, Iowa 50011, USA*
(Received 4 August 2009; revised manuscript received 15 December 2009; published 19 January 2010)

First-principles molecular dynamics simulations are performed to investigate the atomic size and chemical effects on the short-range order (SRO) in superheated and undercooled Zr-based metallic liquids, Zr_2M (M=Co, Ni, Cu, and Ag). We demonstrate that the local atomic structures in liquids are quite sensitive to the atomic size ratio and the electronic interactions between component elements. The large negative heats of mixing for Zr-M do not favor icosahedral SRO in these binary liquids, contrary to the common belief. Full icosahedral structure units are few in the superheated liquids, although the number of icosahedral clusters increases upon undercooling. Comparing Zr_2Co, Zr_2Ni, and Zr_2Cu, all of which have very similar atomic size ratios, we find that the degree of local icosahedral order increases with decreasing interaction strength between the d electrons in Zr-Co, Zr-Ni, and Zr-Cu. A comparison of Zr_2Cu and Zr_2Ag alloys shows that the degree of icosahedral order increases much more in Zr_2Ag than in Zr_2Cu with decreasing temperature. The difference in atomic sizes of Cu and Ag may account for the subtle discrepancy in the evolution of short-range ordering in undercooled Zr_2Cu and Zr_2Ag liquids.

DOI: 10.1103/PhysRevB.81.014108 PACS number(s): 61.25.Mv, 61.20.Ja, 31.15.A−

I. INTRODUCTION

Short-range order (SRO) in superheated and undercooled liquids is of great importance to understand crystallization and glass formation as well as the properties of the liquid itself. As first suggested by Frank,[1] an icosahedral short-range order (ISRO) with fivefold symmetry has been widely proposed as the local structure unit responsible for the stability of deeply supercooled metallic liquids and the formation of metallic glasses.[2–6] However, nonicosahedral SRO has also been reported. For example, a bcc-like SRO for elemental Zr liquids was found in *ab initio* molecular dynamics (MD) simulation studies[7] and a polytetrahedral SRO was inferred in Al-Co and Al-Ni metallic alloy liquids.[8]

It has been shown that small isolated clusters often energetically favor distorted, instead of perfect, icosahedral structures.[9–12] It was argued that the cluster geometry is determined by two competing factors:[6,13,14] (a) geometrical factors that maximize the packing density and (b) electronic interactions that minimize the energy. In the presence of strong bonding, the local order of the metallic liquid may deviate from, or become completely different from, ISRO. For multicomponent alloy liquids, the study of SRO becomes even more complex since the interactions between different atom pairs may be quite different, giving rise to a tendency of chemical short-range order (CSRO).[15] The dominant SRO will therefore be determined by both geometrical and chemical ordering effects, wherein the latter may enhance or disfavor ISRO.[14,15]

Despite the extensive experimental and theoretical efforts, satisfactory understanding of the SRO in metallic liquids still remains a challenge at the present time, more comprehensive studies of deliberately selected alloy systems are necessary to get insights into the exact nature of SRO. Binary alloys, due to their relative simple structures, are often selected as model systems to study the atomic structures of liquid and amorphous alloys. In this paper, we address the important issue of the SRO in the liquid alloys and its evolution in the undercooled region through a systematic comparative first-principles MD simulations and analysis (including the electronic-structure analysis) of four prototype Zr-based binary alloys, Zr_2M (M=Co, Ni, Cu, and Ag). The effects of the atomic size was investigated by comparing the SRO in Zr_2Cu and Zr_2Ag alloys, and the effects of electronic interactions was probed by comparing the local atomic and electronic structures in Zr_2Co, Zr_2Ni, and Zr_2Cu alloys. Here we note that metallic radius of Ag is larger than Cu (1.44 Å for Ag and 1.27 Å for Cu)[16] and have similar chemical interactions as Cu with the matrix component Zr; Co, Ni, and Cu atoms are in the same row of periodic table, thus of similar metallic radius (1.25 Å for Co and Ni)[16] but with different electronic configurations ($3d^74s^2$ for Co, $3d^84s^2$ for Ni, and $3d^{10}4s^1$ for Cu), thus giving rise to different chemical properties. Results from our simulation studies show that the large negative heats of mixing for Zr-M do not favor icosahedral SRO in these binary liquids. This finding corrects a prevailing empirical rule in the discussion on metallic glass formation from the undercooled liquids. We show clearly how the local atomic structures in metallic liquids are related to the atomic size ratio and the electronic interactions between component elements. In particular, we show that the degree of ISRO in these liquids is strongly correlated with the density of states (DOS) of the d electrons of the M elements near the Fermi level.

The paper is arranged as follows. In Sec. II, the technical details of the *ab initio* MD simulations will be described. The simulation results are presented and discussed in Sec. III. The resulting atomic structures are characterized by their pair-correlation functions (PCFs), chemical order parameters,[17] Voronoi polyhedra indices,[18] Honeycutt and

TABLE I. Number densities (atoms/Å^3), partial nearest-neighbor distances R_{ij} (Å), partial coordination numbers Z_{ij}, and chemical order parameters η_{ij} in superheated and undercooled Zr_2M (M=Co, Ni, Cu, and Ag) liquids.

Alloy	T (K)	ρ_0	$R_{Zr\text{-}Zr}$	$R_{Zr\text{-}M}$	$R_{M\text{-}M}$	$Z_{Zr\text{-}Zr}$	$Z_{Zr\text{-}M}$	$Z_{M\text{-}Zr}$	$Z_{M\text{-}M}$	$\eta_{Zr\text{-}Zr}$	$\eta_{Zr\text{-}M}$	$\eta_{M\text{-}M}$
Zr_2Co	1830	0.0508	3.20	2.60	2.42	10.71	4.21	8.42	1.86	−0.03	0.10	−0.29
	1283	0.0517	3.20	2.62	2.54	10.20	4.37	8.74	1.02	−0.07	0.19	−0.58
Zr_2Ni	1673	0.0506	3.18	2.65	2.54	9.83	4.35	8.71	2.28	−0.04	0.10	−0.26
	1173	0.0514	3.20	2.67	2.57	10.50	4.26	8.53	1.70	−0.04	0.12	−0.35
Zr_2Cu	1648	0.0490	3.16	2.77	2.49	9.84	4.05	8.10	2.43	−0.02	0.06	−0.16
	1156	0.0499	3.10	2.73	2.49	10.18	4.18	8.37	2.32	−0.03	0.07	−0.20
Zr_2Ag	1894	0.0439	3.15	2.94	2.72	9.23	4.04	8.08	4.65	0.03	−0.06	0.13
	1328	0.0448	3.13	2.97	2.81	9.45	4.11	8.23	3.91	0.01	−0.02	0.04

Andersen (HA) indices,[19,20] and bond orientational order (BOO) parameters.[2,21] The electronic structures are studied through the analysis of partial density of states of the Zr and M elements, respectively. Finally, a summary is given in Sec. IV.

II. COMPUTATIONAL DETAILS

Our first-principles calculations were performed within density-functional theory using plane-wave basis, with the projector-augmented-wave (PAW) method for core-valence electron interactions,[22,23] as implemented in VASP code.[24] The electronic exchange and correlation potential is described within the generalized gradient approximation (GGA) due to Perdew and Wang (PW91).[25] Default plane-wave cutoffs from the PAW-GGA database are used in calculations.

The MD simulations were carried out in the canonical ensemble (NVT) with Nóse thermostats to control the temperature. Newton's equations of motion were integrated using the Verlet algorithm with a time step of 3 fs. A cubic cell containing 99 atoms was used with periodic boundary conditions. Only the Γ point was used to sample the Brillouin zone in the MD simulations, whereas in the calculations of electronic density of states, a $2\times2\times2$ Monkhorst-Pack k-point meshes were used. The average pressure of the system at each temperature was tuned to a value close to zero by changing the size of the supercell. Two temperatures were considered for each alloys. One is in the superheated liquid, above the experimental melting temperature T_m, $T=1.29T_m$, and the other is in the undercooled region, $T=0.91T_m$. In order to eliminate any "memory" effect from the initial configuration, the systems were thermalized at a temperature of 2500 K for 3 ps. After the liquid was thermally equilibrated at the elevated temperature, the systems were gradually cooled down to the temperature $1.29T_m$ with a cooling rate of 0.05 K/step. An additional 4000 MD steps was performed to collect the atomic trajectories to study the structures and properties of the liquids after equilibration. Subsequently, this procedure was repeated for the other temperature $0.91T_m$, starting from the previous configurations at $1.29T_m$. The structural properties of the undercooled states are then calculated by performing the statistical averages over 5000 MD steps.

III. RESULTS AND DISCUSSION

The atomic number densities of the superheated and undercooled liquids produced by these treatments are presented in Table I. The values for Zr_2Ni liquids (0.0506 atoms/Å^3 at 1673 K and 0.0514 atoms/Å^3 at 1173 K) have been found to be in good agreement with the experimental values, which are equal to 0.0505 and 0.0516 atoms/Å^3, respectively.[26] To our best knowledge, the number densities of the other three liquids are not available from experiments to compare with the results from our *ab initio* MD simulations. By analyzing the atomic trajectories from the simulations described above, we have obtained several structural quantities of interest as well as their evolution upon undercooling.

A. Pair distribution function $g(r)$

As a first step, we have considered the total PCF, $g(r)$, which is an important physical quantity to characterize the structure of liquids due to its direct connection with experimental results. It is defined to be proportional to the density of atoms at a distance r from another atom. Using the atomic coordinates from the MD simulations, the total PCFs for the four binary liquid alloys at the superheated and undercooled states are calculated and presented in Figs. 1(a) and 1(b), respectively. As can be seen in Fig. 1(a), the height of the first peak in the total $g(r)$ increases in the order of Zr_2Co, Zr_2Ni, Zr_2Cu, and Zr_2Ag, and the troughs between the first and second peaks become deeper at the same time, indicating an increasing degree of SRO. The positions of the peaks in the $g(r)$ also shift slightly toward the larger r value in the same order; In Fig. 1(b), the peaks are sharper while the locations are virtually unchanged with undercooling. The trend is still the same as that in the superheated liquids. Moreover, the splitting in the first peak of the total $g(r)$ for the undercooled Zr_2Co and Zr_2Ni can be clearly observed.

The partial PCFs for the four systems are also shown in Figs. 2(a)–2(d), respectively. The nearest-neighbor bond lengths, estimated from the first maxima of each of the partial PCFs are also compiled in Table I. From Fig. 2 and Table I, we can make the following observations: (1) in all the systems studied here, the bond length between Zr-Zr pairs is the longest, the atomic distance between M-M pairs is the shortest, and the distance between unlike atoms are in be-

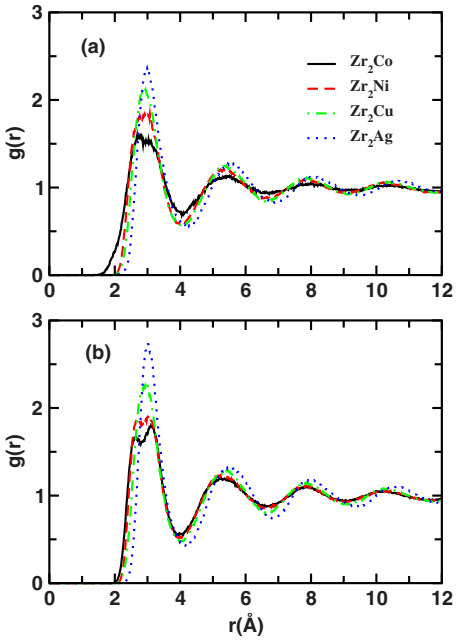

FIG. 1. (Color online) Total pair-correlation functions of (a) superheated and (b) undercooled liquids.

tween; (2) the first peak of $g_{\text{Zr-}M}$ is higher than $g_{\text{Zr-Zr}}$ and $g_{M\text{-}M}$ in Zr_2Co, Zr_2Ni, and Zr_2Cu, suggesting that the interaction between unlike atoms are stronger than Zr-Zr or *M*-*M* while the height of the first peaks of $g_{\text{Ag-Ag}}$ is larger than $g_{\text{Zr-Zr}}$ and $g_{\text{Zr-}M}$, with the latter two are almost equal in Zr_2Ag. (3) The above finding can also be examined by comparing the atomic distances between Zr-Zr (*M*-*M*) pairs and Zr-*M* pairs in each of these liquids. For the former three alloy liquids, the atomic distances of Zr-Zr (*M*-*M*) pairs are equal or close to the sum of the metallic radii of two Zr (*M*) atoms [3.20 Å(2.5 Å)] while the atomic distance of the Zr-*M* pairs is much smaller than the sum of the metallic radii of Zr and *M* atoms (1.60+1.25=2.85 Å) and increases on progressing from Zr_2Co to Zr_2Ni to Zr_2Cu. For Zr_2Ag, the atomic distances between Ag-Ag pairs are also smaller than the sum of the metallic radii of the two Ag atoms (2.88 Å). (4) The height of the peaks of the PCFs increases when quenched to the undercooled states, whereas the peak positions change only slightly, except for $g_{\text{Co-Co}}$, where the amplitude of first oscillation decreases and the amplitude of the second oscillation increases as the temperature decreases. This feature of $g_{\text{Co-Co}}(r)$ corresponds to a decrease in the number of Co neighbors around each Co atom and indicate that Co atoms are most likely repelling each other, which might also contribute to the splitting of the first peak of the total PCF of Zr_2Co. (5) The right-hand side of the second peaks of the partial $g_{M\text{-}M}(r)$'s develops a prominent shoulder in the undercooled liquids, suggesting that *M*-*M* interactions play an important role in the evolution of the local structures upon undercooling. We further note that the shoulder is enhanced the most, actually to higher than the second peak, for $g_{\text{Cu-Cu}}(r)$, followed by $g_{\text{Ag-Ag}}(r)$, which presents a flat shape in combination with the second peak, and then $g_{\text{Ni-Ni}}(r)$ and the least for $g_{\text{Co-Co}}(r)$.

According to the partial PCFs given above, the average nearest-neighbor coordination number (CN), Z_{ij}, can be determined by integrating the radial distribution function $4\pi r^2 \rho g_{ij}(r)$, where ρ is the number density, up to the first minimum of $g_{ij}(r)$. The calculated results are reported in Table I. From Table I, the CN around Zr atom ($Z_{\text{Zr-Zr}}+Z_{\text{Zr-}M}$) is much larger than that around *M* atom ($Z_{M\text{-Zr}}+Z_{M\text{-}M}$) in the four alloy liquids. The difference in CNs around Zr and *M* atoms is plausible due to the difference of their atomic sizes. However, the $Z_{\text{Zr-}M}$ scales with the known heats of mixing for these Zr_2M systems, −41, −49, −23, and −20 KJ/mol for Zr-Co, Zr-Ni, Zr-Cu, and Zr-Ag, respectively.[27] This would suggest that the bond strength may be a more important factor than size. Upon undercooling, the changes of partial CN Z_{ij} are system dependent, suggesting different local chemical ordering in the four liquids. Particularly, $Z_{\text{Co-Co}}$ is much smaller in the undercooled liquid than that in the superheated liquid. This decrease in the number of first neighbors essentially results from the peculiar evolution of partial PCF $g_{\text{Co-Co}}$ with undercooling. In addition, it deserves mentioning that the partial CN $Z_{M\text{-}M}$ increases from $Z_{\text{Co-Co}}$ to $Z_{\text{Ni-Ni}}$ and to $Z_{\text{Cu-Cu}}$, and the averaged CN around Ag is much larger than that around Cu in both the superheated and the undercooled liquids. We emphasize here that the former trend just results from the different chemical interaction strength between Zr and *M* (*M*=Co, Ni, and Cu) and the latter from the atomic size difference between Ag and Cu. Note that the atomic size ratio of $R_{\text{Ag}}/R_{\text{Zr}}$ is 0.900, which is very close to the ideal ratio of 0.902 for an ideal icosahedral dense packing[28,29] while the atomic size ratio of $R_{\text{Co(Ni)}}/R_{\text{Zr}}$ is 0.781, and $R_{\text{Cu}}/R_{\text{Zr}}$ is 0.793. From this aspect, the icosahedral packing would be topologically more efficient in Zr_2Ag than that in Zr_2Cu
alloy.

B. Chemical order parameters

To obtain a more quantitative estimate for the CSRO in the four binary-alloy liquids, we describe the degree of chemical ordering using the chemical order parameters η_{ij} generalized by Cargill and Spaepen.[17] Here, $\eta_{ij}=Z_{ij}/Z^*_{ij}-1$, where Z^*_{ij} is the partial CN in the case of complete chemical disorder. $\eta_{ij}<0$ means the chemical preference against *ij* nearest-neighbor pairs while $\eta_{ij}>0$ means preference for *ij* nearest-neighbor pairs. The calculated chemical order parameters for the four superheated and undercooled liquids are listed in Table I. All the liquids considered here show more or less some degree of chemical ordering with nonzero η_{ij}. As can be seen in Table I, the chemical order parameters between like atoms are *negative* and those between unlike atoms are *positive* in Zr_2Co, Zr_2Ni, and Zr_2Cu, reflecting a heterocoordinating tendency in these liquids. However, this is not the case for Zr_2Ag in which both Zr and Ag atoms show homocoordinating tendency. Notably, $\eta_{\text{Co-Co}}$ and $\eta_{\text{Zr-Co}}$ of the undercooled Zr_2Co liquid have the largest negative (~−0.58) and positive values (~0.19) among these parameters, indicating the strongest heterocoordinating order of Co in the Zr_2Co liquid. These results are consistent with the PCFs and CNs discussed above. Therefore, the SRO in the four binary systems depends on a subtle interplay between chemical and geometrical effects.

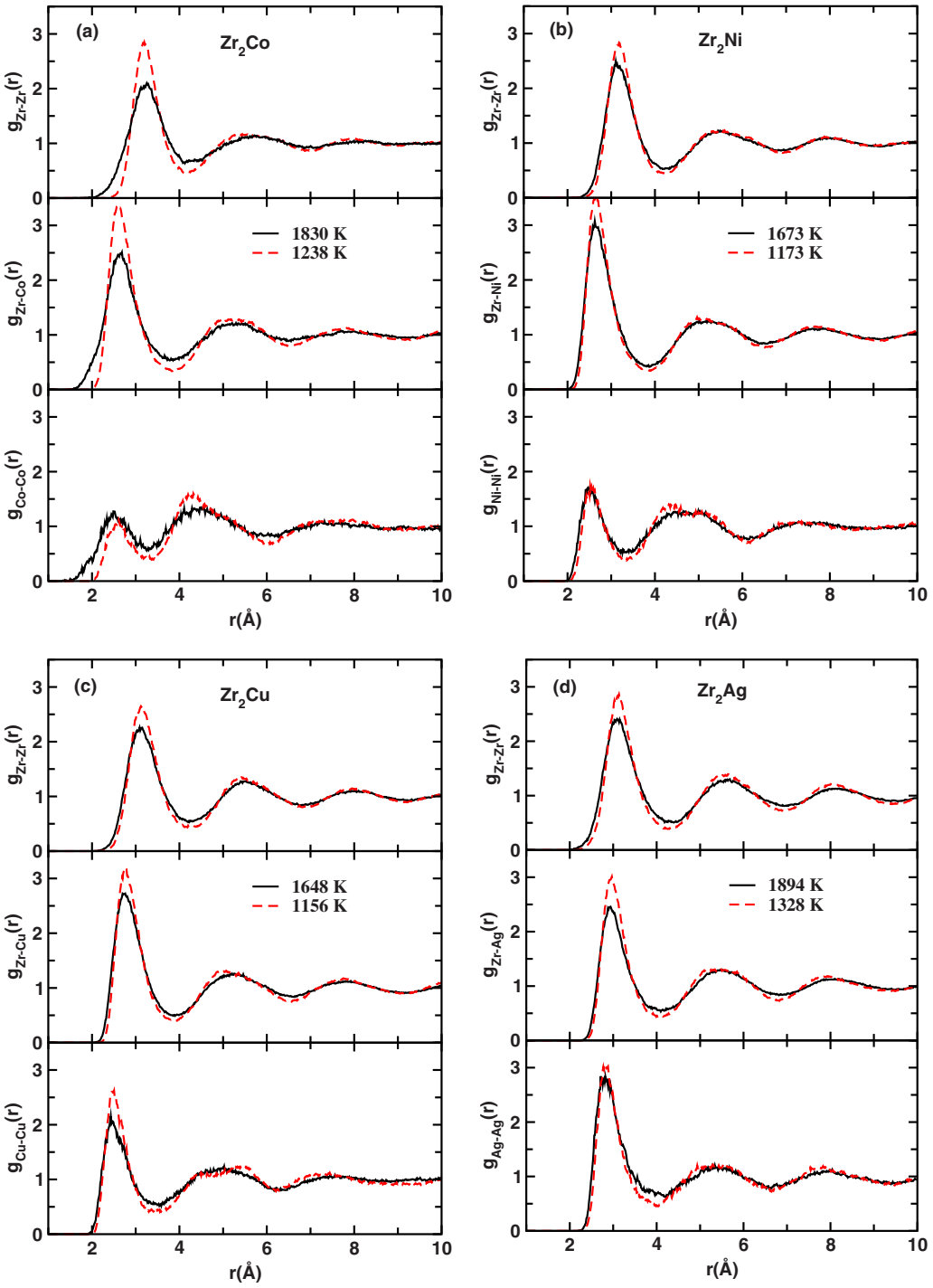

FIG. 2. (Color online) Partial pair-correlation functions for (a) Zr_2Co, (b) Zr_2Ni, (c) Zr_2Cu, and (d) Zr_2Ag liquids at superheated and undercooled states.

C. Honeycutt-Anderson analysis

Next, we use the common-neighbor analysis by HA index[19,20] to obtain a three-dimensional description of the local atomic configuration of the binary-alloy liquids. This method is able to characterize the local environment surrounding each atomic pair that contributes to the peaks of $g(r)$. A set of four indices is assigned to each atomic pair. The first index denotes to what peak the root pair belongs; the second index represents the number of near neighbors shared by the root pair; the third index is the number of bonds among the common neighbors; and a fourth index is used to distinguish the arrangement of the bonds. Here the first minima in the corresponding partial PCFs are chosen to be the cutoff distances, same as in our earlier CN calculations.

The relative abundance of the selected main bonded pairs for the four binary-alloy liquids are listed in Table II. Presented are 1551 index, characteristic of icosahedral short-

TABLE II. HA index pair fractions for 1551's (icosahedral), 1541 and 1431's (distorted icosahedral), 1421 and 1422's (fcc/hcp), and 1661 and 1441's (bcc) in superheated and undercooled Zr_2M (M=Co, Ni, Cu, and Ag) liquids.

	Zr_2Co		Zr_2Ni		Zr_2Cu		Zr_2Ag	
Pairs	1830 K	1283 K	1673 K	1173 K	1648 K	1156 K	1894 K	1328 K
1551	0.22	0.26	0.20	0.30	0.20	0.29	0.20	0.28
1541+1431	0.25	0.34	0.30	0.27	0.39	0.34	0.34	0.36
1421+1422	0.04	0.06	0.06	0.03	0.09	0.05	0.07	0.06
1661+1441	0.19	0.18	0.15	0.22	0.14	0.19	0.15	0.16

range order, 1541 and 1431 indices, characteristic of distorted icosahedral (DICOS) local order, 1441 and 1661 indices, characterizing bcc ordering (bcc), and 1421 and 1422 indices, representative of fcc and hcp ordering, respectively (fcc/hcp).[20] The quantities are normalized such that the total number of pairs contributing to the first peak of the PCF is unity. All the superheated or undercooled liquids studied here contain a substantial amount of the DICOS (~25–40 %), whereas the contribution of 1551 pairs is less (~20–30 %). As we will show later, the actual fraction of local icosahedral order (characteristic of a 13 atom icosahedron) should be much smaller than the weight of the 1551 pairs, which are just the principal structural motifs associated with pentagonal bipyramids. bcc and fcc/hcp-like order are also present but only in small proportions (~15–20 % or less).

The HA index presented in Table II indicates that the SRO in the four Zr-based binary liquids are dominated by pentagonal bipyramid motifs and the amount of these motifs increases with undercooling. These motifs can be considered as fragments or building blocks of icosahedrons. To reveal how these motifs with fivefold symmetry are packed in the four alloy liquids, we further examined how many 1551 (or 1551+1541+1431) pairs n can each atom form with the other atoms on its first neighbor shell. The histogram of 1551 pairs packing around each atom in these liquids at the superheated and undercooled states are presented in Figs. 3(a) and 3(b), respectively. In the superheated liquids, a negligible fraction of atoms form twelve 1551 pairs with their neighbors, which means the perfect icosahedrons would be rare in the high-temperature liquids. In the undercooled liquids, the fraction of the atoms associated with twelve 1551 pairs increases. Here, we note that the fraction of the atoms associated with twelve 1551 pairs is the highest in Zr_2Ag and then followed by Zr_2Cu, Zr_2Ni, and Zr_2Co. When 1541 and 1431 pairs (which are distorted fivefold symmetry structures) are also included, as shown in Figs. 4(a) and 4(b), the proportion of the atoms with n (n is the number of 1551+1541+1431 pairs around each atom) less than 6 decreases with undercooling while the proportion with $n \geq 8$ increases simultaneously. This observation means that the motifs with regular or distorted pentagonal symmetry show a gathering tendency in the undercooled liquids with decreasing temperature, implying that the fragments of local icosahedral order grow with undercooling. It is worthwhile to note that the trend becomes even more clear that Zr_2Ag has the largest degree of ISRO, followed by Zr_2Cu, Zr_2Ni, and the least in Zr_2Co at the undercooled state. Again, these subtle differences of the SRO in the four liquids may be ascribed to the different electronic interactions between the alloying species and the atomic size difference between Ag and Cu.

D. Bond orientational order-parameter analysis

The BOO parameter analysis introduced by Steinhardt *et al.*[2,21] provides another indication of the local structural order in liquids. A set of order parameters expressed in terms of spherical harmonics $Q_{lm}(r)=Y_{lm}[\theta(r)\varphi(r)]$ are associated with the orientation of each pair of atoms. To account for equivalent structures that are oriented differently, the rotationally invariant combination is used,

$$Q_l = \left[\frac{4\pi}{2l+1} \sum_{m=-l}^{l} |\bar{Q}_{lm}|^2 \right]^{1/2}.$$

Different structures are characterized by Q_l's of different intensities.

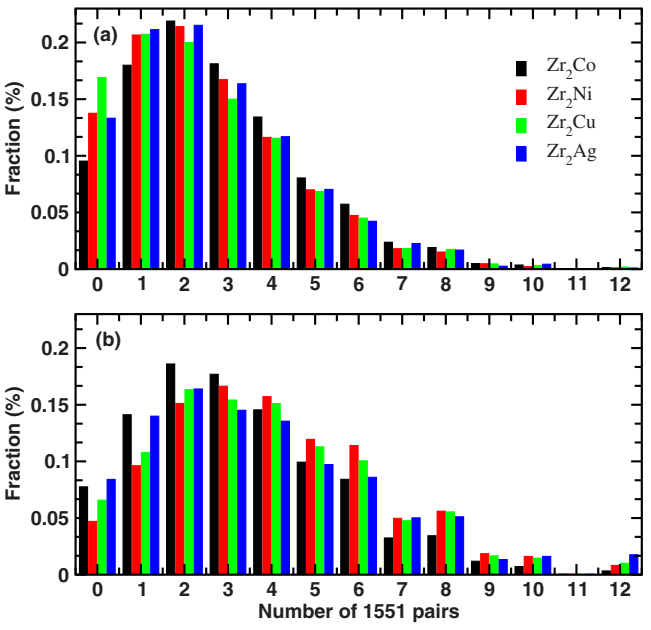

FIG. 3. (Color online) Distribution of HA 1551 pairs in (a) superheated and (b) undercooled Zr_2Co, Zr_2Ni, Zr_2Cu, and Zr_2Ag liquids.

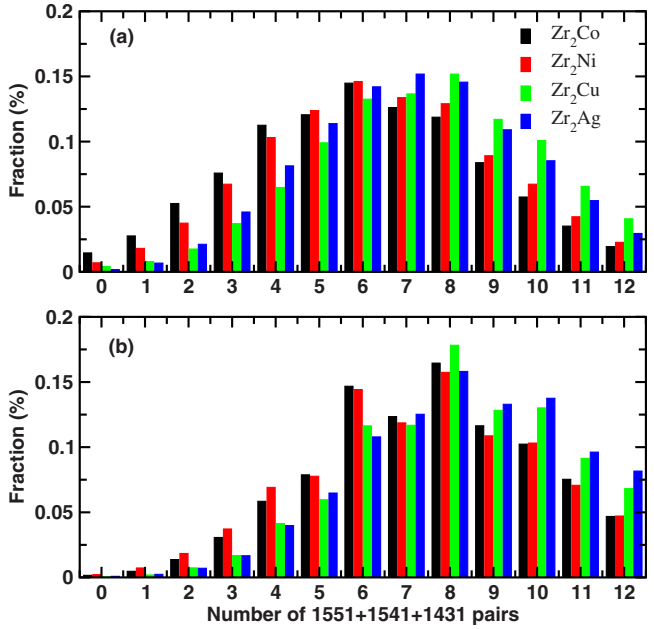

FIG. 4. (Color online) Distribution of HA 1551, 1541, and 1431 pairs in (a) superheated and (b) undercooled Zr_2Co, Zr_2Ni, Zr_2Cu, and Zr_2Ag liquids.

Figure 5 shows the BOO results for the four superheated and undercooled liquids. The Q_l's are calculated for neighboring atoms. As before, we choose the first minima of the partial PCFs to the cutoff distances to specify near neighbors.

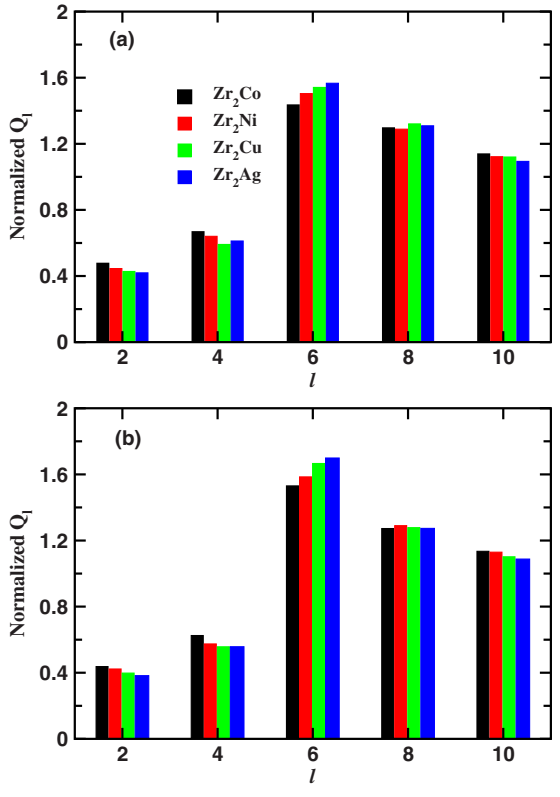

FIG. 5. (Color online) Normalized BOO analysis of (a) superheated and (b) undercooled Zr_2Co, Zr_2Ni, Zr_2Cu, and Zr_2Ag liquids.

Each set of Q_l's was multiplied by a factor to give a normalized sum of 5 ($\Sigma_{evenl}Q_l=5$), the normalized sum for a random configuration. All of the normalized Q_l's are nonzero, indicating an orientational ordering in liquids. The even-l spherical harmonics are considered here since they are most useful for characterizing the angular correlations within the local structure.[30] With undercooling, the intensity of normalized Q_l changes differently for different values of l in those liquids. It is interesting to note that the normalized value of Q_6 *increases* in the undercooled liquids while the values for other indices decreases or show only a minimal change, suggesting growing icosahedral ordering with undercooling.[2,21] A comparison between the four liquids shows that different degrees of ISRO are present in these liquids, as already observed from the HA index analysis. Particularly, Q_6 has the largest value in undercooled Zr_2Ag liquids, followed by Zr_2Cu, Zr_2Ni, and the least in Zr_2Co, indicating the strongest ISRO in Zr_2Ag liquid.

E. Voronoi analysis

The atomic structures were further analyzed by Voronoi tessellation method.[18] In this method, the perpendicular bisectors between a central atom and all of its neighboring atoms will form a polyhedron about the central atom, which can be differentiated by specific Voronoi indices $\langle n_3,n_4,n_5,\ldots\rangle$, where n_i denotes the number of i-edged faces of the Voronoi polyhedron. The total number of the faces of the Voronoi polyhedron equals to the CN of the central atom.

Figures 6(a)–6(d) show the fraction of the 20 most abundant Voronoi indices that appear in the four liquids in the superheated and undercooled states, respectively. The indices are arranged in order of increasing coordination of the central atoms. From Fig. 6, one can see that different types of Voronoi clusters exist around Zr and M atoms in those liquids. Among these various types of Voronoi clusters, only several indices appear with high frequencies and show large increase with undercooling, signaling the evolution of some special ordering in the liquid structures; The Zr-centered Voronoi clusters prefer a higher CN than the M-centered clusters due to the larger atomic size of Zr. The four systems show several features: (1) the number of Voronoi cluster types is the smallest in Zr_2Ag and increases in the order of Zr_2Cu, Zr_2Ni, and Zr_2Co. These results indicate that the degree of SRO in terms of Voronoi polyhedra are the strongest in Zr_2Ag and the weakest in Zr_2Co liquids. (2) Distribution of the atomic CNs becomes narrower from Zr_2Co to Zr_2Ni to Zr_2Cu to Zr_2Ag. It ranges from 10 to 16 for Zr_2Co, 11 to 16 for Zr_2Ni and Zr_2Cu, and 12 to 15 for Zr_2Ag. Furthermore, Voronoi indices with the same CNs for Zr- and Ag-centered clusters are well mixed in Zr_2Ag alloy liquids while the mixing degree decreases from Zr_2Cu to Zr_2Ni, and the indices for Zr- and Co-centered clusters are well separated in Zr_2Co liquids with the low CN clusters being exclusively Co centered. (3) The Voronoi index $\langle 0,0,12,0\rangle$ associated with perfect icosahedral clusters is within the top 20 indices for the undercooled Zr_2Cu and Zr_2Ag liquid, and represents 1.10% and 2.03% of the whole Voronoi index population while in Zr_2Co and Zr_2Ni undercooled liquids, the fractions of

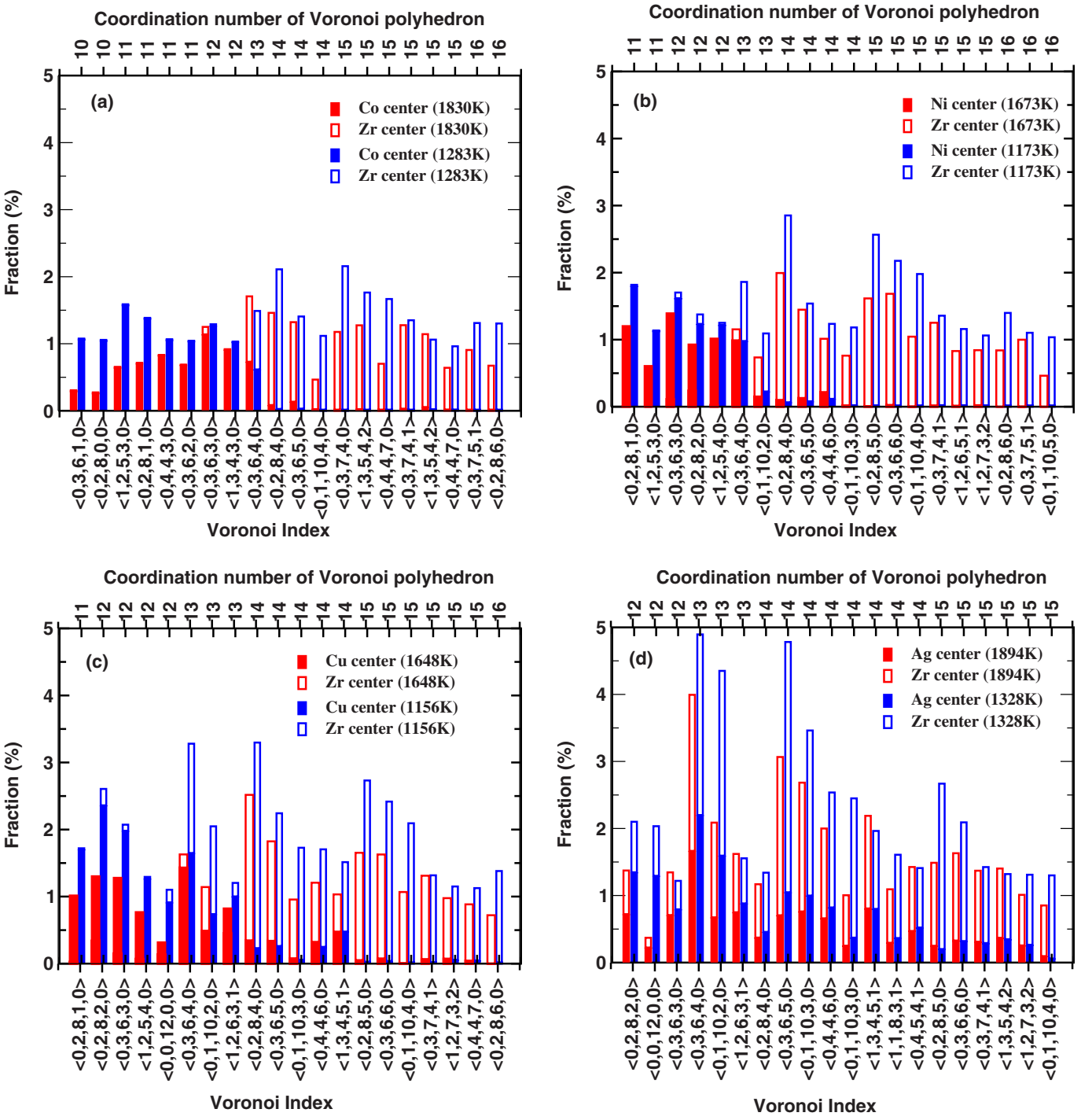

FIG. 6. (Color online) Populations of the 20 most frequent Voronoi indices for (a) Zr_2Co, (b) Zr_2Ni, (c) Zr_2Cu, and (d) Zr_2Ag liquids at superheated and undercooled states. The indices are sorted by the CN as shown in the top of the figures.

$\langle 0,0,12,0\rangle$ are negligible small, only 0.07% and 0.29%, respectively. (4) In spite of the fact that the number of icosahedral clusters with Voronoi index of $\langle 0,0,12,0\rangle$ is small in all the systems, the Voronoi indices related to some form of distorted icosahedral structures such as $\langle 0,1,10,2\rangle$, $\langle 0,2,8,2\rangle$, and $\langle 0,3,6,3\rangle$ still represent a large population, and again show a decreasing trend from Zr_2Ag to Zr_2Cu to Zr_2Ni, and to Zr_2Co, in full agreement with previous HA and BOO analysis.

We note that all the structural properties reported above are produced based on the MD trajectories. To uncouple the vibrational motion from the underlying structural properties, inherent structures[31] have also been studied by rapid quenching of ten snapshots regularly spaced in time for each undercooled liquid. The representative inherent structure samples are shown in Fig. 7. HA indices, BOO parameters, and Voronoi analysis have been performed on the inherent structures. The structural trends of these four binary liquids ob-

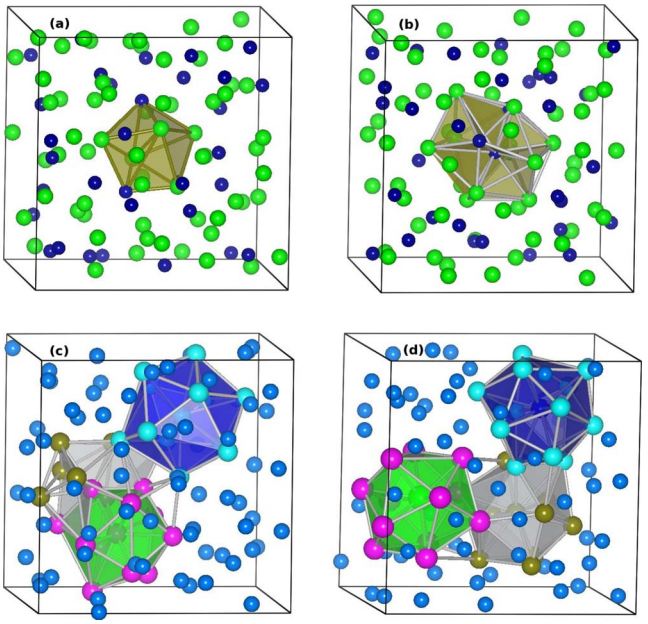

FIG. 7. (Color online) Representative inherent structure of the undercooled liquid (a) Zr_2Co, (b) Zr_2Ni, (c) Zr_2Cu, and (d) Zr_2Ag. The big and small balls in (a) and (b) represent Zr and Co (Ni) atoms, respectively. Polyhedron in (a) indicates a bipyramid unit. Polyhedron in (b) is an icosahedron. In (c) and (d), the red, gold and cyan balls represent the vetex atoms belonging to three different icosahedral clusters.

served in the high-temperature simulations become even more pronounced in the inherent structures. For example, the fraction of $\langle 0,0,12,0\rangle$ in the inherent structures (averaged over ten configurations for each liquid) becomes 3.54% for Zr_2Ag, 3.03% for Zr_2Cu, and 0.61% for Zr_2Co while decreases to zero for Zr_2Co. As can be seen in Fig. 7, bipyramid units (155 HA pairs with their common neighbors) can be identified in the inherent structure of the undercooled Zr_2Co liquid but no perfect icosahedral clusters present. For Zr_2Ag, three icosahedral clusters consisting of 35 atoms exist in the inherent structure sample of 99 atoms. Since entropy contributes significantly to stabilize the liquids at high temperatures, it is worthwhile mentioning that inherent structure could be very different from the liquid structure at high temperatures.

F. Electronic-structure analysis

It is evident from the above discussions that the electronic structure have significant influence on the atomic structure in the Zr-based binary liquids. We now perform analysis of the role of chemical interaction in these liquid alloys. The partial DOS of Zr and M (M=Co, Ni, Cu, and Ag) in undercooled liquids are presented in Fig. 7. The DOS of superheated Zr_2M liquids are not shown as they are similar to those of the undercooled liquids. The results presented here are obtained by averaging over DOS generated from ten snapshots taken during the course of a 15 ps MD simulation for each liquid.

As shown in Fig. 8, the most prominent feature of the electronic structures is a substantial amount of local DOS at the Fermi level derived from the d bands of Zr, which predominantly contribute to the chemical interactions with the d electrons of M atoms, leading to directional chemical bonding between Zr and M atoms. It is interesting to note that the d states of the M atoms are shifted to lower energies and become narrower from Co to Ni to Cu. The amount of d electrons near the Fermi level is most in Zr_2Co, less in Zr_2Ni, and the least in Zr_2Cu. In addition, comparing the DOS of elemental Cu to Ag, one can see that the d states of Ag is deeper and wider than that of Cu, and Ag has even less electrons than Cu around the Fermi level, although atomic Ag and Cu have the same valence electronic configurations. These results imply that the directional bonding strength of Zr-Co is the strongest, with that of Zr-Ni, and then that of Zr-Cu smaller and the bond strength Zr-Ag being the weakest. Our calculation results suggest that directional bonding from the interactions between the d electrons of Zr and M elements suppress the icosahedral SRO in these systems. The strength of directional bonding is anticorrelated with the degree of icosahedral SRO in these systems and also account for the fact that the bond length increases from Zr-Co to Zr-Ni to Zr-Cu to Zr-Ag and all are much smaller than the sum of their metallic radii, as clearly shown in their partial $g_{ij}(r)$'s. The decrease in ISRO also anticorrelates with heat of mixing in these alloys. The fact that Zr_2Co has slightly less ISRO than Zr_2Ni even though Zr-Ni has the slightly higher heat of mixing suggests that size does play a small effect. Zr_2Ag has the highest ISRO, weakest d-electron interaction, lowest ΔH_{mix} and from a hard-sphere packing argument, most geometrically favored to form ISRO. This demonstrates that at least for these systems, strong negative heats of mix-

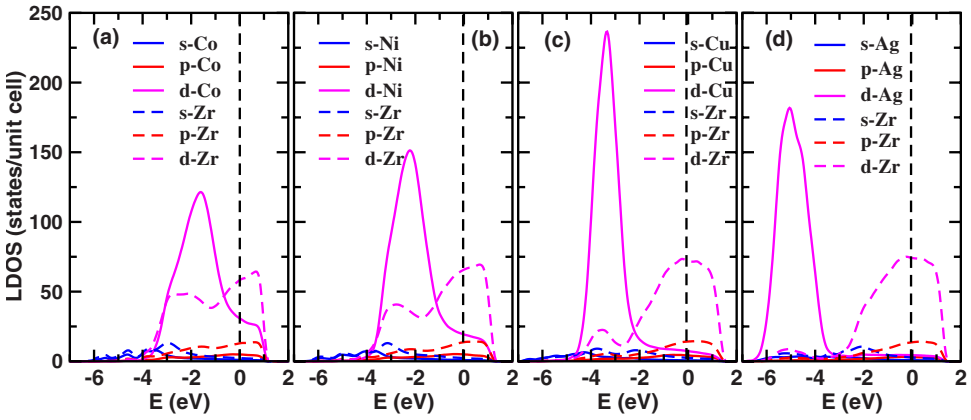

FIG. 8. (Color online) Local density of states for undercooled (a) Zr_2Co, (b) Zr_2Ni, (c) Zr_2Cu, and (d) Zr_2Ag liquids. The Fermi energy is shifted to zero.

ing do not favor ISRO, as has been proposed for metallic glass formation.[32]

IV. SUMMARY

In conclusion, we have performed a systematic comparative *ab initio* MD simulations of Zr-based binary-alloy liquids, Zr_2M (M=Co, Ni, Cu, and Ag). The structure of the superheated and undercooled liquids at the atomic level have been characterized through the pair distribution functions, chemical order parameters, Honeycutt and Andersen indices, Voronoi polyhedra indices, and bond orientational order parameters. Electronic structure and chemical bonding in the liquids have also been studied by analyzing the partial DOS of Zr and M (M=Co, Ni, Cu, and Ag) in liquids. The results from our studies reveal several interesting features:

(1) Intermixing between Zr and M elements is favorable in the Zr_2Co, Zr_2Ni, and Zr_2Cu liquid as one can see from partial pair-correlation functions presented in Fig. 2 where the first peak in partial pair-correlation functions of Zr-M is always stronger than that of Zr-Zr and M-M for these three liquids. This intermixing tendency can also be seen from the chemical order parameter analysis as shown in Table I where the chemical order parameters are all positive for the Zr-M and all negative for Zr-Zr and M-M, respectively, in these three liquids. It should also be noted that the intermixing tendency is strongest in Zr_2Co, followed by Zr_2Ni, and then Zr_2Cu. This tendency is strongly correlated with the strength of the d electrons of the metal atoms at the vicinity of the Fermi level as shown in Fig. 7. These results are consistent with the large negative heats of mixing for Zr-M observed in experiment. On the other hand, the intermixing tendency in Zr_2Ag liquid is weaker than in the Zr_2Cu liquid although both liquids have similar d-electron bonding strength at the Fermi level. This difference can be attributed to the atomic size difference between the two elements.

(2) There are substantial atoms in these liquids arranged in a seven-atom pentagonal bipyramid unit with HA index of 1551, 1541, and 1431 (distorted pentagonal bipyramid). The fraction of the pair of atoms with these two HA indices in these liquids is about 1/3 and does not show a clear trend from one liquid to others. In literature, the fraction of 1551, 1541, and 1431 HA indices are commonly used as the indicator of icosahedral SRO in metallic liquids and glasses. Our present study show that cautions must be taken for such an identification because analysis using Voronoi tessellation method show that the fraction of 13 atom icosahedral clusters (with Voronoi index of $\langle 0,0,12,0\rangle$ and $\langle 0,1,10,2\rangle$ for distorted icosahedral) are very low in these liquids, although the fraction of 1551, 1541, and 1431 HA indices are very high. Our study indicates that the pentagonal bipyramids may only be the fragments of the distorted ISRO. In addition to the population of the 1551, 1541, and 1431 HA, the packing distribution of these pentagonal bipyramids around a common vertex atom as show in Fig. 4 should give more comprehensive information about the degree of the ISRO in the system. Larger number (less or equal to 12) of the pentagonal bipyramids packed around a common vertex will indicate the high degree of icosahedral SRO.

(3) In contrast to the empirical rule in discussion on metallic glass formation from the undercooled liquids, the large negative heats of mixing for Zr-M do not favor strong ISRO in these binary liquids. For example, the degree of ISRO is the weakest in Zr_2Co, followed by Zr_2Ni, Zr_2Cu, and then the highest in Zr_2Ag but the chemical interaction between Zr-M is strongest in Zr_2Co among these four systems. The contrasting evolution behavior of the geometrical and chemical ordering in these undercooled liquid alloys is quite related to the atomic size ratio and the electronic interactions between the component elements. The general trends revealed in the SRO of these binary liquid alloys enable a deeper understanding of liquid structures and their role in metallic glass formation, especially in the absence of high quality atomistic structural data in literature for metallic liquid alloys.

ACKNOWLEDGMENTS

Work at Ames Laboratory was supported by the U.S. Department of Energy, Basic Energy Sciences, including a grant of computer time at the National Energy Research Supercomputing Center (NERSC) in Berkeley, under Contract No. DE-AC02-07CH11358.

[1] F. C. Frank, Proc. R. Soc. London, Ser. A **215**, 43 (1952).
[2] P. J. Steinhardt, D. R. Nelson, and M. Ronchetti, Phys. Rev. Lett. **47**, 1297 (1981).
[3] T. Schenk, D. Holland-Moritz, V. Simonet, R. Bellissent, and D. M. Herlach, Phys. Rev. Lett. **89**, 075507 (2002).
[4] W. K. Luo, H. W. Sheng, F. M. Alamgir, J. M. Bai, J. H. He, and E. Ma, Phys. Rev. Lett. **92**, 145502 (2004).
[5] K. F. Kelton, G. W. Lee, A. K. Gangopadhyay, R. W. Hyers, T. J. Rathz, J. R. Rogers, M. B. Robinson, and D. S. Robinson, Phys. Rev. Lett. **90**, 195504 (2003).
[6] G. W. Lee, A. K. Gangopadhyay, K. F. Kelton, R. W. Hyers, T. J. Rathz, J. R. Rogers, and D. S. Robinson, Phys. Rev. Lett. **93**, 037802 (2004).
[7] N. Jakse and A. Pasturel, Phys. Rev. Lett. **91**, 195501 (2003).
[8] O. S. Roik, O. V. Samsonnikov, V. P. Kazimirov, and V. E. Sokolskii, J. Mol. Liq. **145**, 129 (2009).
[9] F. A. Reuse, S. N. Khanna, and S. Bernel, Phys. Rev. B **52**, R11650 (1995).
[10] J. Y. Yi, Phys. Rev. B **61**, 7277 (2000).
[11] S. Y. Wang, W. H. Duan, D. L. Zhao, and C. Y. Wang, Phys. Rev. B **65**, 165424 (2002).
[12] S. N. Khanna, B. K. Rao, and P. Jena, Phys. Rev. B **65**, 125105 (2002).
[13] G. W. Lee, A. K. Gangopadhyay, R. W. Hyers, T. J. Rathz, J. R. Rogers, D. S. Robinson, A. I. Goldman, and K. F. Kelton, Phys. Rev. B **77**, 184102 (2008).

[14] F. Q. Guo, S. J. Poon, and G. J. Shiflet, J. Appl. Phys. **97**, 013512 (2005).
[15] N. Jakse, O. Lebacq, and A. Pasturel, Phys. Rev. Lett. **93**, 207801 (2004); J. Chem. Phys. **123**, 104508 (2005).
[16] O. N. Senkov and D. B. Miracle, Mater. Res. Bull. **36**, 2183 (2001).
[17] G. S. Cargill III and F. Spaepen, J. Non-Cryst. Solids **43**, 91 (1981).
[18] J. L. Finney, Proc. R. Soc. London, Ser. A **319**, 479 (1970); Nature (London) **266**, 309 (1977).
[19] J. D. Honeycutt and H. C. Anderson, J. Phys. Chem. **91**, 4950 (1987).
[20] A. S. Clark and H. Jónsson, Phys. Rev. E **47**, 3975 (1993).
[21] P. J. Steinhardt, D. R. Nelson, and M. Ronchetti, Phys. Rev. B **28**, 784 (1983).
[22] P. E. Blöchl, Phys. Rev. B **50**, 17953 (1994).
[23] G. Kresse and D. Joubert, Phys. Rev. B **59**, 1758 (1999).
[24] G. Kresse and J. Furthmüller, Comput. Mater. Sci. **6**, 15 (1996).
[25] Y. Wang and J. P. Perdew, Phys. Rev. B **44**, 13298 (1991).
[26] S. G. Hao, M. J. Kramer, C. Z. Wang, K. M. Ho, S. Nandi, A. Kreyssig, A. I. Goldman, V. Wessels, K. K. Sahu, K. F. Kelton, R. W. Hyers, S. M. Canepari, and J. R. Rogers, Phys. Rev. B **79**, 104206 (2009).
[27] F. R. de Boer, R. Boom, W. C. M. Mattens, A. R. Miedema, and A. K. Niessen, *Cohesion in Metals* (North-Holland, Amsterdam, 1988).
[28] T. Egami and Y. Waseda, J. Non-Cryst. Solids **64**, 113 (1984).
[29] D. B. Miracle, J. Non-Cryst. Solids **342**, 89 (2004).
[30] A. Baranyai, A. Geiger, P. R. Gartrellmills, K. Heinzinger, R. Mcgreevy, G. Palinkas, and I. Ruff, J. Chem. Soc., Faraday Trans. 2 **83**, 1335 (1987).
[31] F. H. Stillinger and T. A. Weber, Science **225**, 983 (1984).
[32] A. Takeuchi and A. Inoue, Mater. Trans. **46**, 2817 (2005).